European Journal of Cell Biology 103 (2024) 151398

Contents lists available at ScienceDirect

European Journal of Cell Biology

journal homepage: www.elsevier.com/locate/ejcb

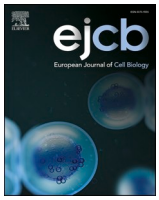

Molecular mechanisms of naringenin modulation of mitochondrial permeability transition acting on F_1F_O-ATPase and counteracting saline load-induced injury in SHRSP cerebral endothelial cells

Salvatore Nesci [a,*], Cristina Algieri [a], Matteo Antonio Tallarida [c], Rosita Stanzione [d], Saverio Marchi [e], Donatella Pietrangelo [k], Fabiana Trombetti [a], Luca D'Ambrosio [f], Maurizio Forte [d], Maria Cotugno [d], Ilaria Nunzi [e], Rachele Bigi [g], Loredana Maiuolo [b], Antonio De Nino [b], Paolo Pinton [h,i], Giovanni Romeo [j], Speranza Rubattu [d,k]

[a] Department of Veterinary Medical Sciences, University of Bologna, Ozzano Emilia 40064, Italy
[b] Department of Chemistry and Chemical Technologies, University of Calabria, Cosenza 87036, Italy
[c] RINA Consulting - Centro Sviluppo Materiali SpA, Via di Castel Romano 100, Rome, 00128, Italy
[d] IRCCS Neuromed, Pozzilli 86077, Italy
[e] Department of Clinical and Molecular Sciences, Marche Polytechnic University, Ancona 60126, Italy
[f] Department of Medical-Surgical Sciences and Biotechnologies, Sapienza University of Rome, Latina 04100, Italy
[g] Department of Neuroscience, Mental Health, and Sensory Organs, Sapienza University, Rome 00189, Italy
[h] Translational Research Center, Maria Cecilia Hospital GVM Care & Research, Cotignola 48033, Italy
[i] Department of Medical Sciences, Laboratory for Technologies of Advanced Therapies (LTTA), University of Ferrara, Ferrara 44121, Italy
[j] Medical Genetics Unit, Sant'Orsola-Malpighi University Hospital, Bologna 40126, Italy
[k] Department of Clinical and Molecular Medicine, Sapienza University of Rome, Rome 00189, Italy

ARTICLE INFO

Keywords:
mitochondria
F_1F_O-ATPase
naringenin
permeability transition pore
ROS
SHRSP

ABSTRACT

Naringenin (NRG) was characterized for its ability to counteract mitochondrial dysfunction which is linked to cardiovascular diseases. The F_1F_O-ATPase can act as a molecular target of NRG. The interaction of NRG with this enzyme can avoid the energy transmission mechanism of ATP hydrolysis, especially in the presence of Ca^{2+} cation used as cofactor. Indeed, NRG was a selective inhibitor of the hydrophilic F_1 domain displaying a binding site overlapped with quercetin in the inside surface of an annulus made by the three α and the three β subunits arranged alternatively in a hexamer. The kinetic constant of inhibition suggested that NRG preferred the enzyme activated by Ca^{2+} rather than the F_1F_O-ATPase activated by the natural cofactor Mg^{2+}. From the inhibition type mechanism of NRG stemmed the possibility to speculate that NRG can prevent the activation of F_1F_O-ATPase by Ca^{2+}. The event correlated to the protective role in the mitochondrial permeability transition pore opening by NRG as well as to the reduction of ROS production probably linked to the NRG chemical structure with antioxidant action. Moreover, in primary cerebral endothelial cells (ECs) obtained from stroke prone spontaneously hypertensive rats NRG had a protective effect on salt-induced injury by restoring cell viability and endothelial cell tube formation while also rescuing complex I activity.

1. Introduction

Mitochondrial dysfunctions affecting the energy production of the cell are involved in a variety of human diseases, especially cardiovascular diseases (CVDs) which are a main cause of death worldwide. Moreover, there is a consensus on the need to increase the prevention of CVDs based on the use of natural products that may delay their onset (Perna et al., 2019). In this regard, the search for new molecules that may counteract mitochondrial dysfunctions related to the risk of CVDs is encouraged by some promising hints coming from the study of

Abbreviations: NRG, naringin; ECs, endothelial cells; QUE, quercetin; SHRSP, stroke prone spontaneously hypertensive rat; MPTP, mitochondrial permeability transition pore; SOX, anion superoxide; CVDs, cardiovascular diseases; PPPCs, polyphenolic phytochemicals; CRC, calcium retention capacity.

* Corresponding author.
E-mail address: salvatore.nesci@unibo.it (S. Nesci).

https://doi.org/10.1016/j.ejcb.2024.151398
Received 14 October 2023; Received in revised form 18 January 2024; Accepted 13 February 2024
Available online 15 February 2024

phytochemical compounds. Phytochemical compounds, which include flavonoids (*e.g.* flavanones) and non-flavonoids (*e.g.* stilbenes) (Fig. 1), are actively studied for their potential to promote healthy life and disease prevention while counteracting chronic diseases (Pérez-Jiménez et al., 2010). In particular, flavonoids are a large family of natural polyphenolic compounds present in common fruits, medical herbs and vegetables with a great variety of therapeutic effects. They have a strong potential to function as free radical scavengers due to their ability to form stable radicals (Sandoval-Acuña et al., 2014). Naringenin (NRG), a flavanone present in the bergamot fruit (*Citrus bergamia*) has received increasing attention due to its broad range of biological activities (Carresi et al., 2020).

Cell protection against radical species by NRG results in a reduction of mitochondrial dysfunction. Moreover, NRG has been reported to reduce acute and chronic inflammatory responses and to exert cardiovascular beneficial properties in clinical trials (Salehi et al., 2019). In particular, the cardioprotective effects of NRG on coronary artery disease, hypertension, cardiac hypertrophy, myocardial infarction and ischemic stroke are most likely due to the hypocholesterolemic, antioxidant, anti-inflammatory and anti-ischemic activities of its flavone structure (Heidary Moghaddam et al., 2020). Nevertheless, studies regarding the precise mechanism of action of NRG in CVDs are lacking and additional efforts should be made to identify the molecular targets of NRG in different cellular contexts and its fine mechanism of action, with special attention to mitochondrial dysfunctions (Carresi et al., 2020).

The mitochondrial dysfunction associated with CVDs is highlighted by an altered cellular energy metabolism caused by an impaired oxidative phosphorylation leading to ATP depletion, increase of oxidative stress and activation of pro-death pathways, which in turn trigger the opening of the mitochondrial permeability transition pore (mPTP) (Bonora et al., 2019). Loss of inner mitochondrial membrane (IMM) permeability, which directly causes mitochondrial swelling, is accompanied by disorders in mitochondrial dynamics (biogenesis, fission and fusion) that usually lead to mitochondrial impairment and degradation (mitophagy) (Forte et al., 2021). Interestingly, the polyphenolic phytochemicals (PPPCs) playing a scavenger action in mitochondria can counteract mitochondrial dysfunction (Algieri et al., 2022a). PPPCs might bind to a common region on the F_1 hydrophilic domain, facing the mitochondrial matrix. They act as F_1 inhibitors and block ATP hydrolysis without overlapping with the three catalytic sites of substrates ADP and Pi, and surprisingly they also confer resistance to mPTP opening (Algieri et al., 2019). NRG, which shares the polyphenolic structure of PPPCs, could itself inhibit ATP hydrolysis and mPTP formation, thus counteracting mitochondrial dysfunctions. However, small molecular differences can produce different biological effects as they may imply distinct chemical interactions with cellular proteins. Therefore, we aimed to test the effects of NRG in endothelial cells of stroke-prone spontaneously hypertensive rats (SHRSP), which offer an excellent model of target organ damage associated with mitochondrial dysfunction (Rubattu et al., 2016a). The NRG beneficial action on the impaired mitochondrial bioenergetics might sustain its use in therapy and address future cardiovascular drug design and development.

2. Material and methods

2.1. Preparation of the mitochondrial fractions

Swine hearts (*Sus scrofa domesticus*) were collected at a local abattoir and transported to the lab within 2 h in ice buckets at 0–4°C. After removal of fat and blood clots as much as possible, approximately 30–40 g of heart tissue was rinsed in ice-cold washing Tris-HCl buffer (medium A) consisting of 0.25 M sucrose, 10 mM Tris(hydroxymethyl)-aminomethane (Tris), pH 7.4 and finely chopped into fine pieces with scissors. Each preparation was made from one heart. Once rinsed, tissues

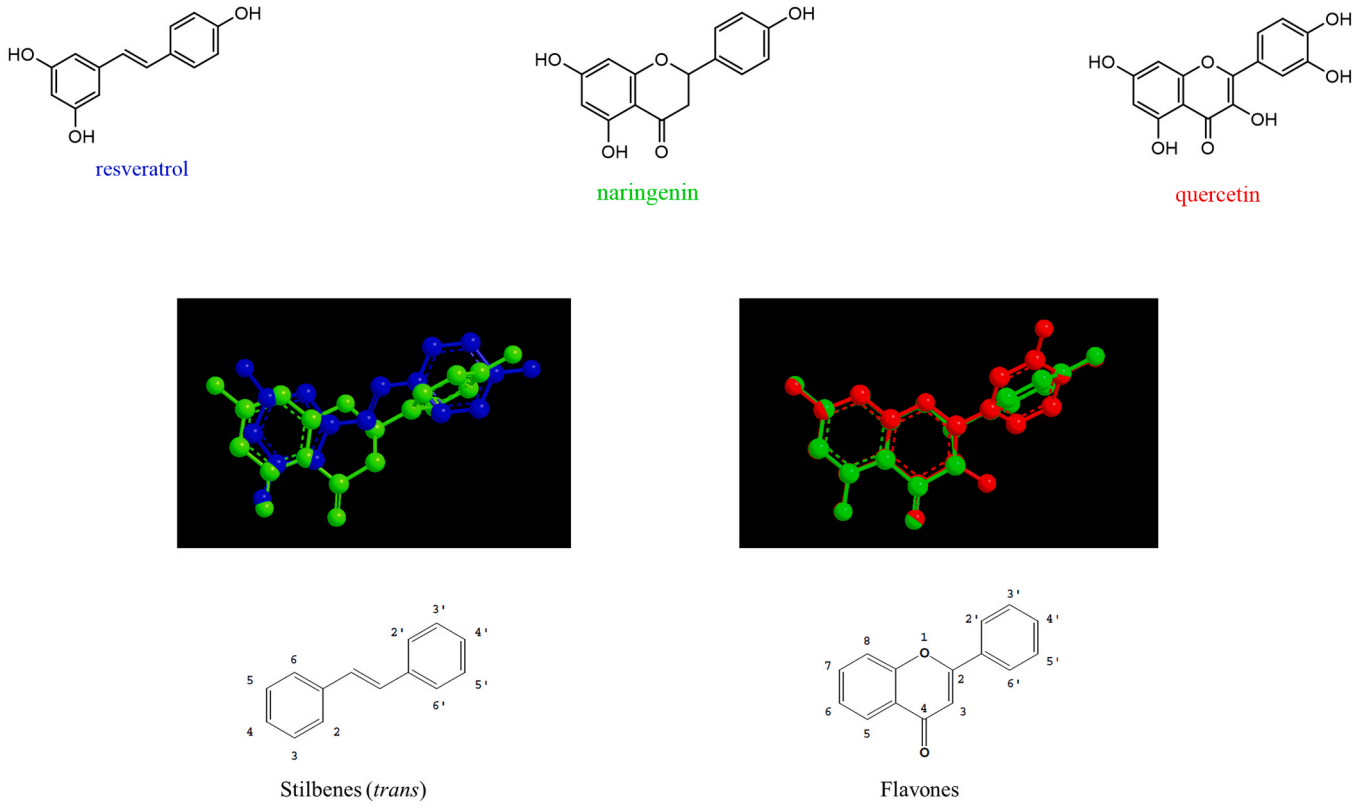

Fig. 1. Molecular structure of resveratrol, naringenin, and quercetin. Overlapping of resveratrol (blu) with naringenin (green) or quercetin (red) with naringenin (green) in the black box on the left or on the right, respectively. The typical structures of stilbene and flavone molecules are depicted.

were gently dried on blotting paper and weighed. Then tissues were homogenized in medium B consisting of 0.25 M sucrose, 10 mM Tris, 1 mM EDTA (free acid), 0.5 mg/mL BSA fatty acid free, pH 7.4 with HCl at a ratio of 10 mL medium B per 1 g of fresh tissue. After a preliminary gentle break-up by Ultraturrax T25, the tissue was carefully homogenized by a motor-driven teflon pestle homogenizer (Braun Melsungen Type 853202) at 650 rpm with 3 up-and-down strokes. The mitochondrial fraction was then obtained by stepwise centrifugation (Sorvall RC2-B, rotor SS34). Briefly, the homogenate was centrifuged at 1,000x*g* for 5 min, thus yielding a supernatant and a pellet. The pellet was re-homogenized under the same conditions as the first homogenization and re-centrifuged at 1,000x*g* for 5 min. The gathered supernatants from these two centrifugations, filtered through four cotton gauze layers, were centrifuged at 10,500x*g* for 10 min to yield the raw mitochondrial pellet. The raw pellet was resuspended in medium A and further centrifuged at 10,500x*g* for 10 min to obtain the final mitochondrial pellet. The latter was resuspended by gentle stirring using a Teflon Potter Elvejehm homogenizer in a small volume of medium A, thus obtaining a protein concentration of 30 mg/mL (Nesci et al., 2014a). All steps were carried out at 0–4°C. The protein concentration was determined according to the colourimetric method of Bradford (Bradford, 1976a) by Bio-Rad Protein Assay kit II with BSA as standard. The mitochondrial preparations were then stored in liquid nitrogen until the evaluation of F_1F_O-ATPase activities.

2.2. F_1 domain purification

After thawing, the mitochondrial suspensions of the swine heart were diluted with 50 mL of medium A to obtain a concentration of 20 mg/mL of protein, sonicated on ice with Sonicator MSE Soniprep 150 to an amplitude of 210 μm for 3 minutes three times with 30 second intervals and centrifuged at 10,000×*g* for 10 minutes. The supernatant from this first centrifugation was further centrifuged at 100,000×*g* for 2 hours. All these centrifugation steps were performed at 4°C. The pellet was resuspended in medium A plus 4 mM Na_2ATP, the pH was adjusted to 9.2 by adding small aliquots of 20% (w/w) NH_4OH solution and stored overnight at 4°C. The next day, the suspension, in which the pH was brought back to 8.0 by adding small aliquots of aqueous solution of 2 N HCl, was sonicated at an amplitude of 210 μm for 5 minutes and then centrifuged at 300,000×*g* for 1 hour (Penin et al., 1979). The resulting pellet was resuspended in 9 mL of medium A plus 2 mM EDTA, pH 7.6. After the addition of 4.5 mL of chloroform, the resulting mixture was vigorously vortexed for 15 seconds and centrifuged at 600×*g* for 10 minutes to allow for separation of the two phases. The upper aqueous phase was collected and further centrifuged at 100,000×*g* for 1 hour. The obtained pale yellow supernatant was supplemented with adequate aliquots of freshly prepared ATP solution to obtain a final 4 mM ATP concentration and with a 2 N NaOH solution to adjust pH to 8.0. After the dropwise addition of saturated solution $(NH_4)_2SO_4$ plus 5 mM EDTA under continuous stirring to obtain a saturation of 37% and a pH adjustment to 8.0 with a 1 N KOH solution (Penin et al., 1979), the suspension was centrifuged at 10,000×*g* for 15 minutes. Pellet was discarded and the collected supernatant was brought to 60% saturation with solid $(NH_4)_2SO_4$; the mixture was then adjusted to pH 8.0 with a 1 N solution of KOH and kept overnight at 4°C (Penin et al., 1979). Finally, pellet from the last centrifugation at 150,000×*g* for 90 minutes, was resuspended by gentle homogenization using a Potter Elvehjem Teflon homogenizer in a small volume of medium containing 100 mM Tris/H_2SO_4, 1 mM EDTA and 50% glycerol, pH 8.0, constituted the partially purified F_1 fraction (Algieri et al., 2019; Penin et al., 1979). Protein concentration was determined according to the Bradford colourimetric method by Bio-Rad Protein Assay kit II using BSA as standard (Bradford, 1976b). Once it was verified that in the partially purified F_1 fraction, ATPase activity, supported by Ca^{2+} or Mg^{2+}, was completely insensitive to 1 μg/mL of oligomycin, thus demonstrating the detachment of the F_O sector, the partially purified F_1 fraction was then preserved in liquid nitrogen and no further purification was carried out.

2.3. Mitochondrial F_1F_O-ATPase activity assays

Thawed mitochondrial preparations were immediately used for F-ATPase activity assays. The capability of ATP hydrolysis was assayed in a reaction medium (1 mL). The optimal conditions to obtain the maximal activity of the F_1F_O-ATPase, which depend on substrates concentration and pH values, are at 0.15 mg mitochondrial protein and 75 mM ethanolamine-HCl buffer pH 9.0, 6.0 mM Na_2ATP and 2.0 mM $MgCl_2$ for the Mg^{2+}-activated F_1F_O-ATPase assay, and 75 mM ethanolamine-HCl buffer pH 8.8, 3.0 mM Na_2ATP and 2.0 mM $CaCl_2$ for the Ca^{2+}-activated F_1F_O-ATPase assay (Algieri et al., 2019; Nesci et al., 2017). These assay conditions were previously proven to elicit the maximal enzyme activities either stimulated by Mg^{2+} or by Ca^{2+} in swine heart mitochondria (Algieri et al., 2020). After 5 min pre-incubation at 37°C, the reaction carried out at the same temperature, was started by the addition of the substrate Na_2ATP and stopped after 5 min by the addition of 1 mL of ice-cold 15% (w/w) trichloroacetic acid (TCA) aqueous solution. Once the reaction was stopped, vials were centrifuged for 15 min at 3500 rpm (Eppendorf Centrifuge 5202). In the supernatant, the concentration of inorganic phosphate (Pi) hydrolyzed by known amounts of mitochondrial protein, which is an indirect measure of F-ATPase activity, was spectrophotometrically evaluated (Nesci et al., 2014b). According to the method employed, to detect the Pi release by the enzymatic reaction, the Pi released independently of the F_1F_O-ATPase activity should be quantified. To this aim, 1 μL from a stock solution of 3 mg/mL oligomycin in dimethylsulfoxide was directly added to the reaction mixture before starting the reaction. The total ATPase activity was calculated by detecting the Pi in control tubes run in parallel and containing 1 μL dimethylsulfoxide per mL reaction system. In each experimental set, control tubes were alternated to the condition to be tested. The employed dose of oligomycin, a specific inhibitor of F-ATPases which selectively blocks the F_O subunit ensured maximal enzyme activity inhibition and was currently used in F-ATPase assays (Algieri et al., 2019).

NRG concentrations used for the analysis were solubilized in DMSO. The control sample contained the same aliquot of the solvent DMSO (≤10 μL) was employed to solubilize the NRG. In all experiments, the F_1F_O-ATPase activity was routinely measured by subtracting, from the Pi hydrolyzed by total ATPase activity, the Pi hydrolyzed in the presence of oligomycin (Nesci et al., 2014a). In all experiments, the F-ATPase activity, either activated by Ca^{2+} as cofactor or by Mg^{2+}, was expressed as μmol Pi•mg protein^{-1}•min^{-1}.

2.4. F_1-ATPase activity assay

Immediately after thawing, partially purified F_1 domains were used for F_1-ATPase activity assays. The capability of ATP hydrolysis was assayed in a reaction medium (1 mL) containing 0.15 mg F_1 purified protein and 75 mM ethanolammine–HCl buffer pH 9.0, 6.0 mM Na_2ATP, and 2.0 mM $MgCl_2$ or 2.0 mM $CaCl_2$ for Mg^{2+}-activated F_1F_O-ATPase and Ca^{2+}-activated F_1F_O-ATPase assays, respectively. The methods and parameters of ATP hydrolysis and Pi detection were the same as those used for the mitochondrial F-ATPase activity assays. The sensitivity to 3 μg/mL oligomycin was tested to verify the detachment of F_O domain (Algieri et al., 2019).

2.5. Kinetic analyses

The inhibition mechanism of NRG on the Ca^{2+}- or Mg^{2+}-activated F_1F_O-ATPases was explored by the graphical methods of Dixon and Cornish-Bowden plots, which complement one another (Cornish-Bowden, 1974). To this aim, the $1/v$ (reciprocal of the enzyme activity v) in Dixon plot or the S/v ratio in Cornish-Bowden plot were plotted as a function of NRG concentration. In all plots the enzyme-specific activity

was taken as the expression of *v*. To build these plots, different experimental sets were designed in which the F-ATPase activity was evaluated in the presence of increasing NRG concentrations at two ATP concentrations, keeping the divalent cofactor (Mg^{2+} or Ca^{2+}) concentration constant or *vice versa*. In these plots and in the definition of the binary or ternary complexes *S* indicates the ATP substrate or divalent cofactor. The values of K_i, which corresponds to the dissociation constant of the *EI* complex were calculated from the abscissa (changed to positive) of the intercept of the straight lines obtained in the Dixon plots. The values of K'_i, which represent the dissociation constant of the ternary *ESI* complex, were calculated as the abscissa (changed to positive) of the intercept of the straight lines obtained in the Cornish-Bowden plots (Algieri et al., 2021).

Kinetic studies have been conducted on the mutual exclusion of different inhibitors on the same F-ATPase activity. These analyses aimed to shed light on the possible interaction on the F_1 domain between compounds NRG and quercetin (QUE). To build Dixon-like graphs, in which reciprocal data on enzymatic activity ($1/v$) (*y*-axis) *versus* NRG (*x*-axis) concentration, F-ATPase activity were plotted was analyzed without and with a specific concentration of QUE and at constant concentration of ATP substrate. According to the graphical method (Yonetani, 1982) employed, when the straight lines show different slopes and intersection points, the enzyme inhibition mirrors the combined effect of two inhibitors. When F-ATPase is inhibited by two non-mutually exclusive compounds, for example, QUE (I_1) plus NRG (I_2), the enzyme can combine with both inhibitors to produce the ESI_1I_2 (Nesci et al., 2014b) quaternary complex. The value of $-\alpha K'_i$, which represents the dissociation constant of the quaternary complex ESI_1I_2, was calculated from the abscissa (changed to positive) of the intersection point of the two lines obtained in the presence and absence of QUE.

2.6. Docking studies

The study was performed using the crystal structure of ATP synthase retrieved from the Protein Data Bank (http://www.rcsb.org/) with PDB code 2JJ2. Molecular docking was performed with AutoDock Vina (Trott and Olson, 2009), by keeping the docking parameters at default values. The geometries of QUE and naringenin (NRG) were previously optimized using quantum mechanics. Geometry optimizations and frequency calculations for stationary point characterization were carried out with Gaussian16 using the M06–2X hybrid functional (Zhao and Truhlar, 2008), the 6–31 G(d,p) basis set, and ultrafine integration grids. Bulk solvent effects in water were considered implicitly through the IEF-PCM polarizable continuum model (Scalmani and Frisch, 2010). The protein structure was processed with AutodockTools-1.5.6rc3 (Morris et al., 2009) to toggle problems of incomplete structures due to missing atoms or water molecules. Ligands and protein structure files were converted to PDBQT (Protein Data Bank Partial Charge and Atom Type) and the docking was executed using the Lamarckian algorithm. The grid box consisted of 25 grid points in all three dimensions (X, Y, and Z) separated by a distance of 1 Å between each one. As for the docking analysis of naringenin over the quercetin-inhibited enzyme a 45×45×45 grid box was chosen in order to allow the alghorithm to find the best docking position in the presence of QUE. For the docking analysis of naringenin over the quercetin-inhibited enzyme a 45×45×45 grid box was chosen in order to allow the alghorithm to find the best docking position in the presence of QUE. The docking protocol was validated by simulating the pose of QUE in the crystal structure, obtaining a low discrepancy between the pose of the docked ligand and the pose of the crystallographic ligand. Such a low discrepancy was assessed by considering a RMSD threshold value of 1.5 Å as done for our previous docking study towards F_1-ATP synthase (C. Algieri et al., 2023). The crystallographic ligand was docked after adding hydrogen atoms with AutodockTools-1.5.6rc3 (Morris et al., 2009) and without optimizing its geometry. For all the simulations, the protein was kept rigid.

2.7. mPTP, membrane potential, and anion superoxide evaluation in mitochondria

Fresh swine heart mitochondria (1 mg/mL) were suspended and energized in assay buffer (130 mM KCl, 1 mM KH_2PO_4, 20 mM HEPES, pH 7.2 with Tris) incubated at 37 °C with 1 μg/mL of rotenone and 5 mM succinate as a respiratory substrate. The opening of mPTP was induced by the addition of low concentrations of Ca^{2+} (20 μM) at fixed time intervals (1 min). Calcium retention capacity (CRC) was evaluated spectro-fluorophotometrically in the presence of 0.8 μM of Fura-FF. The probe has different spectral properties in the absence and presence of Ca^{2+}, *i.e.* it shows excitation/emission spectra of 365/514 nm in the absence of calcium (Fura-FF low Ca^{2+}) and moves to 339/507 nm in the presence of calcium concentrations (Fura-FF high Ca^{2+}). PTP opening, implying a decrease in CRC, was detected by increasing the fluorescence intensity ratio (Fura-FF high Ca^{2+})/(Fura-FF low Ca^{2+}). Membrane potential (Δφ) was evaluated in the presence of 0.5 μM JC-10. In polarized mitochondrial membranes, this probe selectively generates an orange JC-10 aggregate (excitation/emission spectra of 540/590 nm). The JC-10 monomers, generated when Δφ decreases, cause a green shift (excitation/emission spectra of 490/525 nm). Consequently, membrane depolarization (decrease in Δφ) attributed to mPTP formation was detected by the increase in the fluorescence intensity ratio, which corresponds to an increase in the aggregate JC-10/monomers JC-10 ratio (C. Algieri et al., 2023). Anion superoxide (SOX) was detected by mitoSOX Red indicator. The production of superoxide by mitochondria after addition of 1 μM antimycin A was observed as MitoSOX fluorescence intensity (a.u.) increase at absorption/emission spectra of 396/610 nm. 1 mM MgADP was used as mPTP inhibitor (C. Algieri et al., 2023). All measurements were processed by LabSolutions RF software.

2.8. Rat primary cerebral endothelial cells isolation and culture

Primary cerebral endothelial cells (ECs) were isolated, as previously reported (Forte et al., 2020; Stanzione et al., 2023), from SHRSP newborn (1–3 day-old) rat brains by enzymatic and mechanic digestions and subsequent positive selection using microbeads magnetically labeled with CD31 antibody (Miltenyi Biotec, Bergisch Gladbach, Germany). ECs were cultured in DMEM/F12 medium (Thermo Fisher Scientific, Waltham, MA, USA) supplemented with 5% FBS (Euroclone Srl, Pero, Italy) and ECGS (Sigma Aldrich–Merck, Darmstadt, Germany) on gelatin-precoated dishes at 37°C and 5% CO_2 in a humidified incubator. Cells were used between passages 1–4 for all experiments. *In vivo* experiments for EC isolation were performed in accordance with the European Commission guidelines (Dlg 2010/63/EU) and the protocol was approved by the Italian Ministry of Health (protocol n.: 448/2022-PR).

2.9. Cell treatments

ECs were exposed to salt loading as previously reported (C. Algieri et al., 2023; Forte et al., 2020; Stanzione et al., 2023). Different NRG concentrations (10, 20, 30, 40 μM) were tested on cell viability, NAD/NADH ratio (as a measure of complex I activity) and angiogenesis to identify the most suitable dose able to counteract the harmful effects of high salt loading in our cellular model. Therefore, ECs were exposed for 72 hrs to the following treatments: NaCl 20 mM, 10 μM NRG, 20 μM NRG, 30 μM NRG, 40 μM NRG, and 20 mM NaCl + NRG (from 10 to 40 μM). Both NaCl and NRG were diluted in the cell medium. In these experimental conditions, we evaluated the cell proliferation, complex I activity, and angiogenesis as described below.

2.10. Cell proliferation assay

To test the effect of NRG on cell viability, ECs were plated in 96-well plates at a density of 1×10^4 cells/well and, the day after, they were

exposed for 72 hrs to the different concentrations of NRG either in the absence or in presence of NaCl 20 mM. The proliferation evaluation was performed using the quantitative colorimetric MTT (3-(4,5-Dimethylthiazol-2-yl)−2,5-Diphenyltetrazolium Bromide) assay (Sigma Aldrich–Merck). At the end of the treatment, ECs were incubated for 2–3 hrs with 10 μL of MTT reagent (5 mg/mL) in a 37°C, 5% CO_2 incubator. Then, 100 μL of DMSO were added to each well, and the absorbance of the solubilized substrate was measured with a microplate reader (Bio-rad, Hercules, CA, USA) at a wavelength of 570 nm.

2.11. NAD/NADH ratio assay

NAD and NADH levels were measured in ECs by using commercially available colorimetric kits (Abcam ab65348). For this purpose, 1×10^6 EC cells were plated in 100 mm cell culture dishes and then exposed to the chosen concentrations of NRG either in the absence or in presence of NaCl 20 mM for 72 hrs. At the end of the treatment, NAD and NADH values were read at 450 nm by a microplate reader and the NAD/NADH ratio was calculated as reported by the manufacturer's protocol.

2.12. Angiogenesis assay

The angiogenesis assay was performed by using a Matrigel matrix (Corning, Sigma Aldrich-Merck). In the specific, 50 μl of Matrigel matrix were added to each well of a 96-multiwell plates and allowed to solidify for 1 hr at 37°C. To test the effects of NRG on angiogenesis, ECs were exposed for 72 hrs to the different concentrations of NRG either in the absence or in the presence of NaCl 20 mM. At the end of the treatment, 1×10^4 ECs were plated on top of the Matrigel layer and incubated for 3–4 hrs. Images were taken with EVOS Cell Imaging Systems (Thermo Fisher Scientific). The number of master junctions, segments and mashes was considered to evaluate the angiogenesis. These parameters were quantified using a specific plugin "Angiogenesis analyzer" of Image J software (National Institutes of Health, Bethesda, MD, USA) (Carpentier et al., 2020).

2.13. mPTP opening in cells

Experiments were conducted in intact SHRSP cerebral ECs, and mPTP opening has been assessed as mitochondrial membrane potential decay over time upon addiction of 80 mM NaCl. Mitochondrial membrane potential was measured by loading cells with 40 nM tetramethyl rhodamine methyl ester (TMRM) for 45 min at 37 °C and then imaged over time using a 3D Cell Explorer-fluo microscope (Nanolive, Switzerland) as previously described (C. Algieri et al., 2023). Basal levels were normalized on fluorescence in the presence of 10 μM FCCP [carbonyl cyanide 4-(trifluoromethoxy) phenylhydrazone], a protonophore that induces a rapid collapse of the membrane potential.

2.14. Statistical analysis

All values are expressed as mean ± standard error (SEM) or standard deviation (SD). Comparisons between the experimental groups were performed by one-way ANOVA followed by Bonferroni post hoc test or Student–Newman–Keuls test. A P value of <0.05 was considered significant. GraphPad Prism (Ver 5.01 GraphPad Software, Inc., La Jolla, CA, USA) statistical software was used for the statistical analysis.

3. Results

3.1. Effect of the NRG on F_1F_O-ATPase

Dose-response effect of NRG was evaluated on Mg^{2+}- and Ca^{2+}-activated F_1F_O-ATPase. The ATP hydrolysis is supported by a divalent cofactor-dependent way and, in the range of 0.1 μM – 4 mM NRG, different power of inhibition was exerted on the enzyme. NRG displayed a higher inhibition efficiency on Ca^{2+}-activated F_1F_O-ATPase than on Mg^{2+}-activated F_1F_O-ATPase. The maximal concentration of NRG tested (4 mM) inhibits Mg^{2+}- and Ca^{2+}-activated F_1F_O-ATPase by 49% and by 76%, respectively (Fig. 2A and B).

Some polyphenols, such as resveratrol, quercetin, and piceatannol, cause the F_1F_O-ATPase inhibition by non-covalent bond (Gledhill et al., 2007) (Fig. 3A), preventing the mPTP opening (Algieri et al., 2019) and subsequent cell death. To give a clue on the possible molecular interactions of NRG and QUE on F_1F_O-ATPase, we performed several docking analyses by exploiting the crystallographic structure already available in the Protein Data Bank for the quercetin-inhibited enzyme (PDB, link: https://www.rcsb.org/) (see Figure S1 for the details). Such analyses must be considered only valid for the Mg^{2+}-activated condition since the Ca^{2+}-activated F_1F_O-ATPase structure is not available yet. In doing so, we performed a preliminary docking analysis wherein we attempted to reproduce the crystallographic pose of QUE to validate our docking protocol (Figure S1A,B). Then, we performed the docking analysis of NRG within the empty QUE active site, assessing that NRG shows a very similar affinity toward the same site in comparison with QUE (Figure S1C,D).

Lastly, an additional docking analysis was performed over the active site occupied by QUE. Comparable affinity values were obtained for NRG even in this case (Fig. 3B). Therefore, it might be reasonable to propose that NRG could interact near the QUE-active site whilst this latter is present. Of course, it might be reasonable to speculate the other way round (NRG within the QUE-active site), but since a crystallographic structure of F_1-ATPase in complex with NRG is not available, such a docking analysis would be excessively speculative. However, the docking score indicated that the F_1 domain of the enzyme could be a strong NRG target, confirming the interesting features of NRG.

3.2. The inhibition mechanism of NRG revealed by inhibition kinetics analyses

The enzyme-NRG interaction related to the presence or absence of the ATP substrate or cation cofactors (Mg^{2+} or Ca^{2+}) was evaluated by kinetic analysis based on the building of Dixon and Cornish-Boweden plots. The inhibition exerted by NRG on the enzyme showed an uncompetitive mechanism with respect to the ATP substrate for Mg^{2+}- (Fig. 4A,B) and Ca^{2+}-activated F_1F_O-ATPase (Fig. 4C,D). According to the mechanism of uncompetitive inhibition, usually observed when the enzyme has two or more binding sites, NRG binds to a different site than that of the ATP substrate, but only when the enzyme–substrate (*ES*) complex is already formed, in order to yield the enzyme–substrate-inhibitor (*ESI*) complex. Moreover, the dissociation constants of the *ESI* complex known as the K_i' values of the F_1F_O-ATPase were the same for Mg^{2+}- and Ca^{2+}-activated F_1F_O-ATPase (3.11±0.30 mM *vs* 2.90 ±0.21 mM). These K_i' values indicated that NRG formed the ternary complex (enzyme-ATP-NRG) irrespective of the divalent cation which acted as a cofactor.

Studying the inhibition mechanism exerted by NRG on both Mg^{2+}- and Ca^{2+}-activated F_1F_O-ATPase with respect to the divalent cation cofactor (*C*), a mixed-type inhibitory effect was depicted. The mixed-type mechanism indicated that the inhibitor can bind to the free enzyme and form the binary complex *EI* (enzyme-NRG) or the ternary complex *ECI* (enzyme-cofactor-NRG). However, considering the dissociation constants of the *EI* complex (K_i) and the *ECI* complex (K'_i), since Mg^{2+}-activated F_1F_O-ATPase (Fig. 4E,F) showed K_i value (6.30 ±0.48 mM) higher than K'_i value (2.70±0.29 mM), the formation of the ternary complex (enzyme-Mg^{2+}-NRG) was preferred. Conversely, the mixed-type inhibition exerted by NRG on Ca^{2+}-activated F_1F_O-ATPase indicated that the formation of the binary complex (enzyme-NRG) was favoured with respect to that of the ternary complex (enzyme-Ca^{2+}-NRG) displaying a K_i value (1.13±0.05 mM) lower than K'_i value (3.23 ±0.13 mM). On balance, the dissociation constants values were lower in the presence of Ca^{2+} than in the presence of Mg^{2+}, thus pointing out that

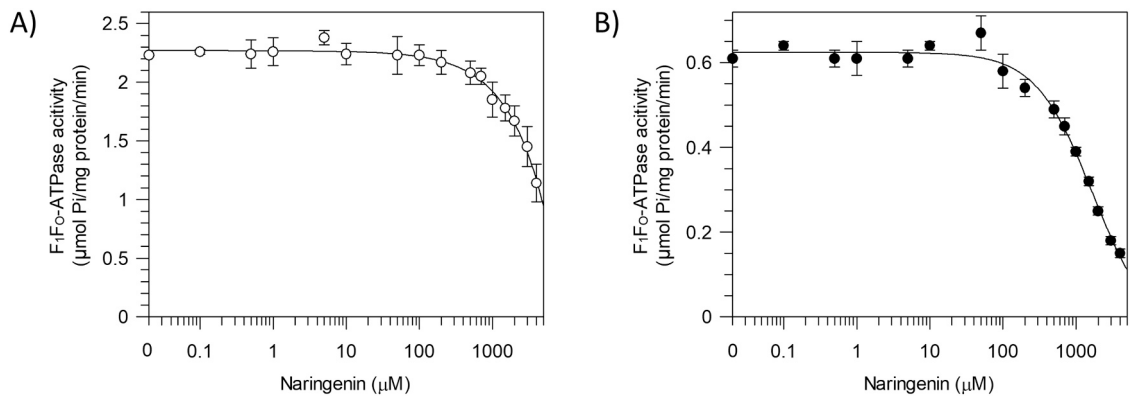

Fig. 2. Response of the mitochondrial Mg^{2+}- and Ca^{2+}-activated F_1F_O-ATPase activities to increasing naringenin concentrations. Data, expressed as ATPase activity of the Mg^{2+}-activated F_1F_O-ATPase (A) and Ca^{2+}-activated F_1F_O-ATPase (B), represent the mean±SD from four independent experiments carried out on different mitochondrial preparations.

NRG preferably binds to Ca^{2+}-activated F_1F_O-ATPase.

3.3. Multiple inhibition analysis on F_1 domain with NRG

To demonstrate the possible interaction of NRG with the hydrophilic F_1 domain of the enzyme, a mutual exclusion analysis approach has been adopted carrying out experiments with binary mixtures of NRG and QUE. The latter is known as an inhibitor of the F_1 domain (Algieri et al., 2019). The tests aimed at clarifying if NRG can combine with the enzyme-QUE complex to form the enzyme-QUE-NRG complex or if the binding of the QUE prevents the binding of the NRG. Thus, we tested if QUE and NRG are mutually exclusive (Fig. 5A,B). The reciprocal of Mg^{2+}- or Ca^{2+}-activated F_1F_O-ATPase activity in the presence and in the absence of fixed QUE concentration was plotted as a function of increasing NRG concentrations. Two straight lines intersecting above the *x*-axis in the presence of Mg^{2+} (Fig. 5A) were obtained. This result depicts a simultaneous interaction of NRG and QUE with the enzyme forming the enzyme-QUE-NRG complex (dissociation constant 1.1 ±0.1 mM). On the contrary, NRG and QUE were mutually exclusive inhibitors in the interaction with Ca^{2+}-activated F_1F_O-ATPase as illustrated by parallel straight lines in which the slopes were independent of the presence or absence of QUE (Fig. 5B). NRG and QUE could not bind simultaneously to the enzyme activated by Ca^{2+}.

To verify that the binding site of NRG is placed on the F_1 domain of the enzyme, the flavone was tested on the purified catalytic portion that performs ATP hydrolysis. The F_1-ATPase activity was insensitive to oligomycin or inhibited by NBD-Cl, which are F_O or F_1 domain-specific inhibitors respectively, in a manner independent from the activation with Mg^{2+} (Fig. 5C) or Ca^{2+} (Fig. 5D) of the purified portion of the enzyme. The tested flavones, QUE and NRG, had a dose-dependent inhibitory effect that was more enhanced on Ca^{2+}-dependent F_1-ATPase rather than on Mg^{2+}-dependent F_1-ATPase.

3.4. Mitochondrial bioenergetics modulated by NRG

By interacting with the F_1 domain, the inhibitory effect of NRG on Ca^{2+}-activated F_1F_O-ATPase was related to a beneficial effect on mitochondrial bioenergetics. The mPTP opening was highlighted by a decreased CRC (Fig. 6A) and the dissipation of mitochondrial $\Delta\varphi$ (Fig. 6B) when a threshold of Ca^{2+} pulse at 1 min intervals triggered the pore formation. As a consequence, the Fura-FF ratio and the JC-10 ratio increased, respectively. NRG blocked the mPTP formation preventing the increase in the Fura-FF ratio or JC-10 ratio. However, 40 µM or 200 µM NRG profiles *vs* Ruthenium Red (RR), an inhibitor of mitochondrial calcium uniporter, profile of CRC were different. The addition of 0.5 µM FCCP decreased the CRC value of control and 40 µM NRG. Conversely, the desensitization of CRC by 200 µM NRG was unaffected by FCCP stimulation (Fig. 6A). The mPTP opening depolarized the mitochondria bypassing the FCCP effect except in the presence of MgADP which inhibited the pore formation. On the contrary, the FCCP addition tpo mitochondria in the presence of MgADP increased the JC-10 ratio emulating the effect of mPTP opening (Fig. 6B). The antioxidant effect of flavonoid structure of NRG was evaluated on the SOX production in mitochondria. Energized mitochondria with substrate for the first site of phosphorylation (complex I-linked substrates: pyruvate plus malate) (Fig. 6C,D) or with substrate for the second site of phosphorylation (complex II-linked substrate: succinate) were tested with two NRG concentrations (40 µM and 200 µM). NRG did not affect the detection of SOX revealed by mitoSOX™ probe in the presence of pyruvate plus malate (Fig. 6C) or succinate (Fig. 6E). Antimycin A added to energized mitochondria stimulated the SOX generation. The increase in mitoSOX intensity antimycin A-dependent by substrates for complex I was mostly decreased at low dose of NRG (Fig. 6D). Conversely, under the condition of succinate respiration blocked with antimycin A, NRG at both tested concentrations had a preventive effect on SOX production (Fig. 6F).

3.5. NRG counteracts the harmful effects induced by saline load in SHRSP primary cerebral ECs

NRG, at doses of 30 and 40 µM, exerted a significant protective effect against the harmful effect of high salt exposure on cell viability (Fig. 7A). On the contrary, NRG alone did not induce any significant effect on cell viability. We investigated mitochondrial function by assessing the activity of mitochondrial complex I. ECs exposed to high-salt loading showed a decreased NAD/NADH ratio, as an index of mitochondrial complex I dysfunction, similarly to what was previously reported in the SHRSP (Forte et al., 2020; Rubattu et al., 2016a), and in *in-vitro* studies (C. Algieri et al., 2023; Stanzione et al., 2023). NRG, at doses from 20 to 40 µM, was able to rescue the complex I activity in ECs exposed to high salt load (Fig. 7B). NRG alone did not induce any significant effect on complex I activity.

NRG at all doses was able to rescue the ECs ability to form vessel-like tubes on a matrigel substrate in the presence of high salt loading (Fig. 7C,D). Interestingly, NRG alone at the dose 10 µM significantly reduced the number of master junctions, of segments and mashes compared to untreated ECs, whereas NRG at the dose of 20 µM reduced only the number of segments and mashes compared to untreated ECs. Notably, acute exposure of SHRSP cells subjected to high salt conditions displays a rapid collapse of mitochondrial membrane potential, as a result of mPTP opening, which is completely prevented by NRG pretreatment (Fig. 7E). Our results suggest that NRG represents a suitable approach to rescue endothelial function, through an improvement of mitochondrial function and by inhibiting mPTP functions, in conditions

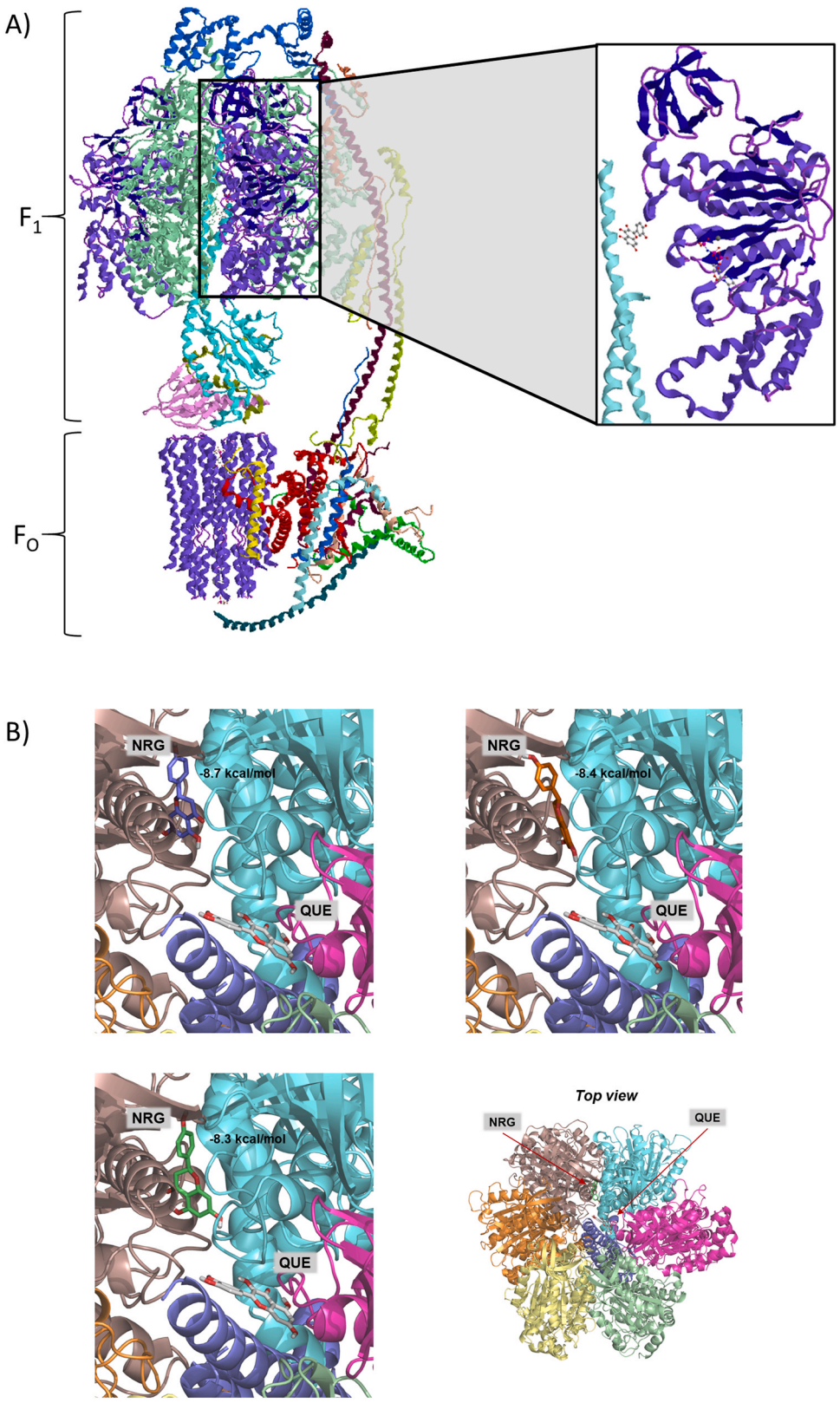

Fig. 3. Docking model of naringenin fitted in the phytochemical compounds binding region of the F_1 domain. A) Structure of F_1F_O-ATPase drawn as ribbon representations obtained from modified PDB ID code: 6TT7. In the box the possible site of naringenin (in ball and stick model) between β (in purple) and γ (in light blue) subunits is highlighted. B) Best three docking poses of naringenin. The docking calculations were performed over the F_1-ATP synthase active site already occupied by quercetin (modified PDB ID code: 2JJ2).

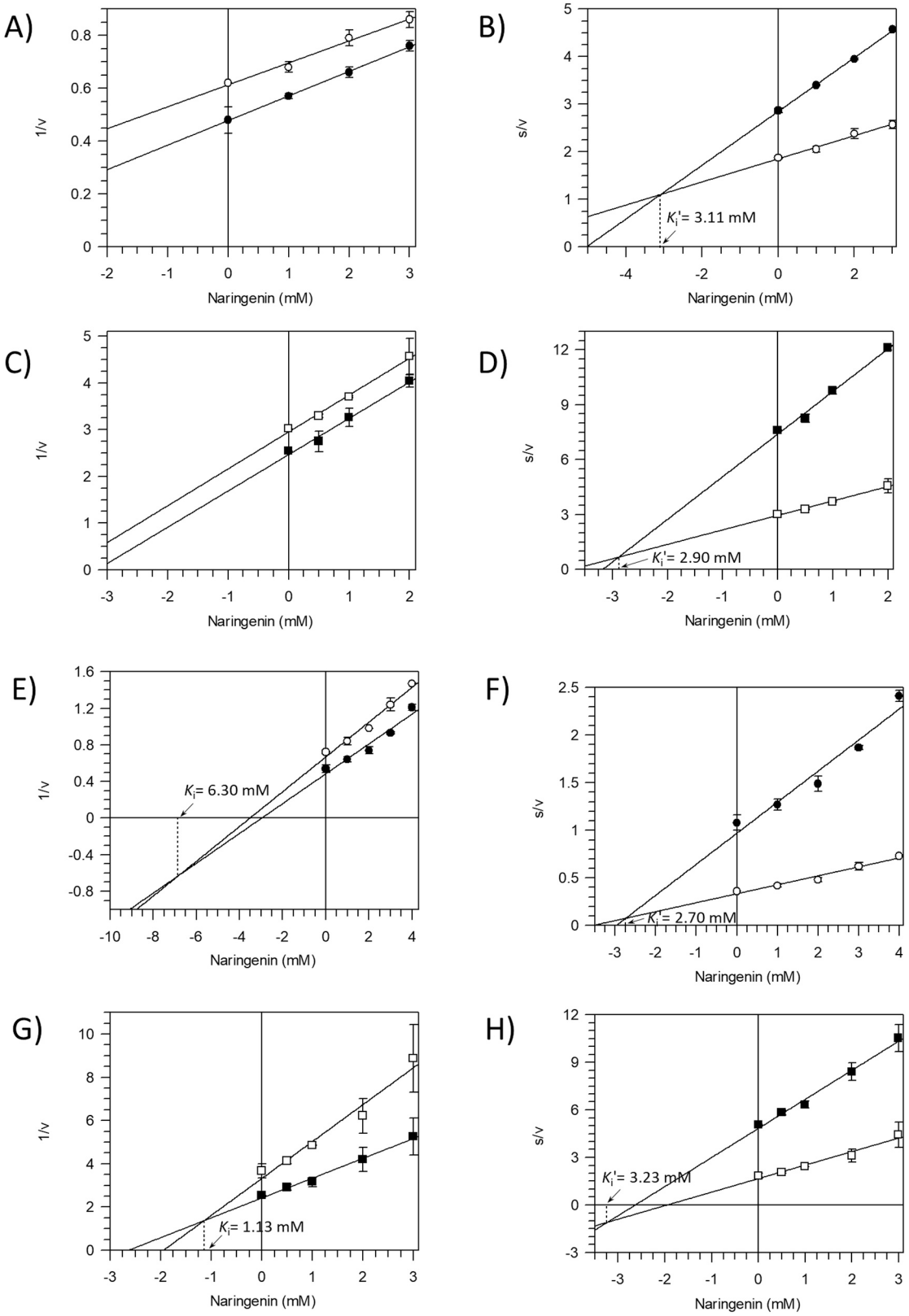

Fig. 4. Inhibition kinetics of the mitochondrial Mg^{2+}- and Ca^{2+}-activated F_1F_O-ATPase activities by naringenin. Dixon (A and C) and Cornish-Bowden (B and D) plots of Mg^{2+}-activated F_1F_O-ATPase at 3 mM ATP (○) or 6 mM ATP (●); and Ca^{2+}-activated F_1F_O-ATPase at 1 mM ATP (□) or 3 mM ATP (■). Dixon (E and G) and Cornish-Bowden (F and H) plots of Mg^{2+}-activated F_1F_O-ATPase at 0.5 mM Mg^{2+} (○) or 2 mM Mg^{2+} (●); and Ca^{2+}-activated F_1F_O-ATPase at 0.5 mM Ca^{2+} (□) or 2 mM Ca^{2+} (■). K_i and K_i' values were obtained as detailed in the kinetic analyses section of Materials and Methods. Each point represents the mean±SD from five experiments on distinct mitochondrial preparations.

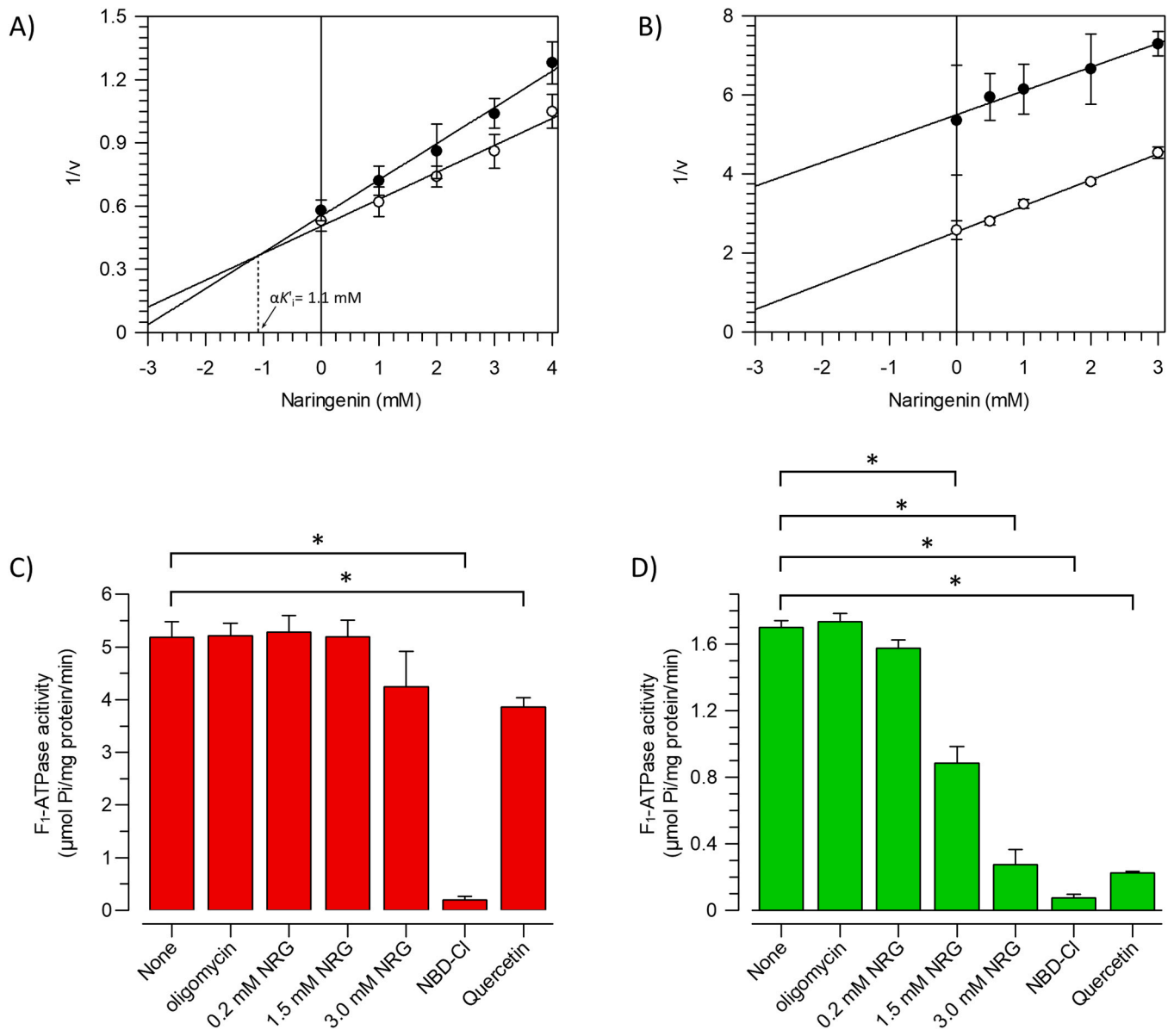

Fig. 5. Effect of naringenin on the F_1 domain. Multiple inhibitor analysis by Dixon plots for Mg^{2+}-activated F_1F_O-ATPase in the presence of 2 mM Mg^{2+} plus 6 mM ATP (A) or Ca^{2+}-activated F_1F_O-ATPase 2 mM Ca^{2+} plus 3 mM ATP (B) inhibition by naringein in the absence (○) or in the presence of 0.4 mM quercetin(●) as detailed in the kinetic analyses section of Materials and Methods 2.4. C) Mg^{2+}- and (D) Ca^{2+}-activated F_1-ATPase activities were evaluated in the absence or in the presence of the inhibitors: 3 µg/mL oligomycin; 0.2 – 1.5 – 3.0 mM naringenin (NRG); 75 µM NBD-Cl; and 0.75 mM quercetin. Each value represents the mean±SD from three independent experiments carried out on distinct F_1 preparations. The asterisk (*) indicates significantly different enzyme activity values ($P<0.05$) in the absence and in the presence of inhibitors.

of high salt-induced injury.

4. Discussion

An impairment of mitochondrial function is linked to CVDs. We investigated the possibility that NRG can resolve the mitochondrial dysfunction caused by the mPTP opening. By acting at the mitochondrial level, NRG may protect from CVDs. In the specific, it may prevent the development of target organ damage in hypertension, a prevalent pathological condition linked to severe cardiac and vascular damage increasing the risk of developing heart failure, myocardial infarction, stroke, and kidney failure (Mollace et al., 2021; Nesci et al., 2023; Rubattu et al., 2015).

The F_1F_O-ATPase has been studied for its features to form the mPTP (Alavian et al., 2014; Bonora et al., 2013). The cryo-EM structure of the enzyme (Pinke et al., 2020) has corroborated the proposed "bent-pull" model in pore formation (Mnatsakanyan and Jonas, 2020). Moreover, the substitution of natural cofactor Mg^{2+} in the catalytic site on β subunits of F_1 domain with Ca^{2+} can trigger a conformational change signal to the membrane-embedded F_O domain to form the mPTP (Giorgio et al., 2017). The link between F_1F_O-ATPase, Ca^{2+} and mPTP (Nesci, 2017) has led to the identification of Ca^{2+}-activated F_1F_O-ATPase as a molecular marker to block mPTP formation (Nesci, 2020). Different small compounds and ions were discovered to be insensitive to Mg^{2+}-activated F_1F_O-ATPase activity but they selectively inhibited Ca^{2+}-activated F_1F_O-ATPase (Algieri et al., 2020, 2019; C. Algieri et al., 2023, 2021; V. Algieri et al., 2023, 2021; Nesci et al., 2021). The phenomenon has been suggested to be linked with the mPTP event (Nesci, 2022; Nesci and Pagliarani, 2021a, 2021b). However, cyclosporine A-sensitive Ca^{2+}-induced permeability transition pore opening is dependent on at least two

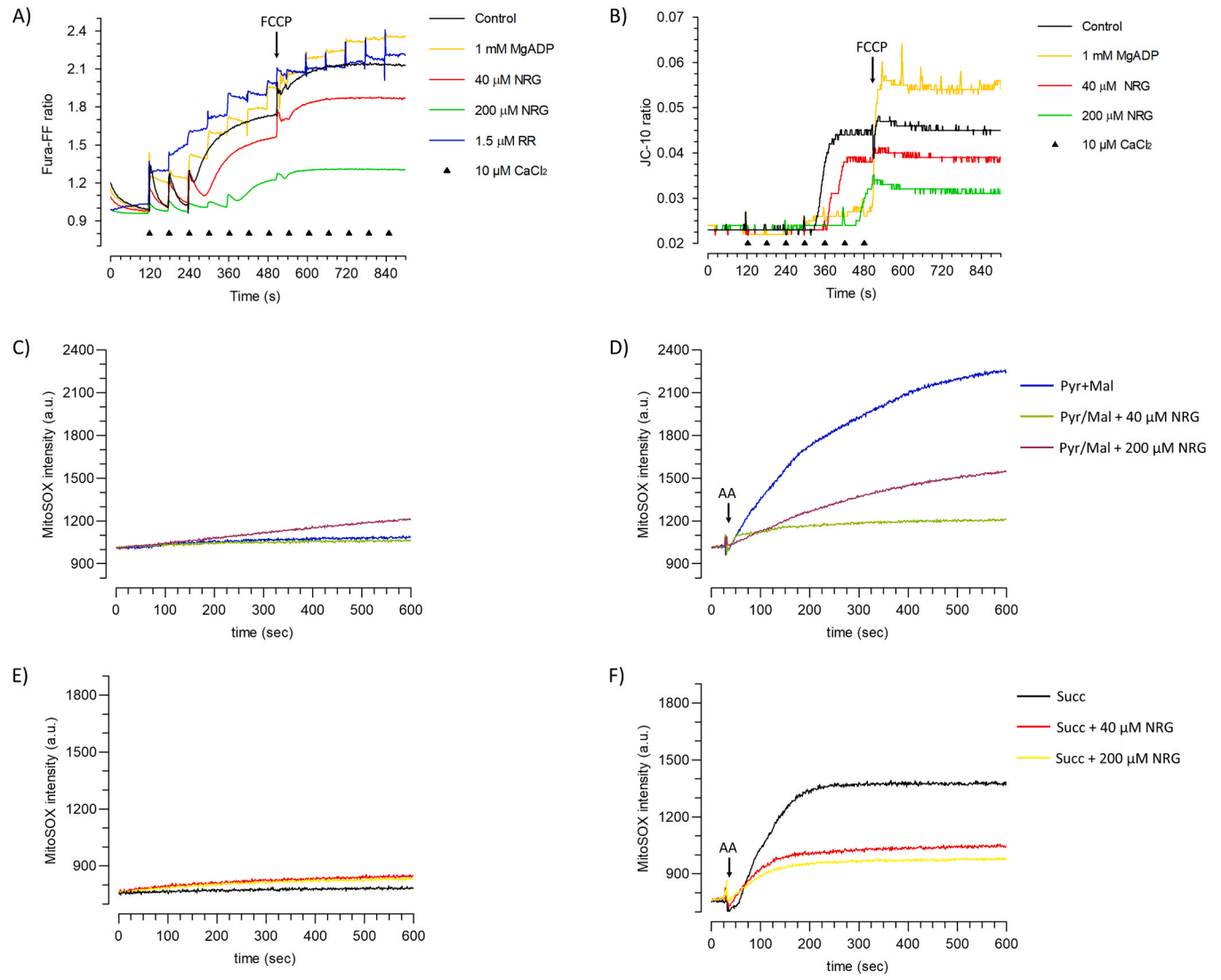

Fig. 6. mPTP opening and ROS production in the presence of naringenin. Representative curves of (A) calcium retention capacity (CRC) expressed as Fura-FF ratio and (B) of the membrane potential expressed as JC-10 ratio to detect the mPTP opening. Evaluation of the anion superoxide production in mitochondria energized with pyruvate plus malate (C and D), substrates for the first site of oxidative phosphorylation (complex I) and with succinate (E and F), the substrate for the second site of oxidative phosphorylation (complex II). The arrow indicates the injection of 0.5 μM FCCP or 1.0 μM antimycin A (AA), an inhibitor of mitochondrial respiration triggering the stimulation of anion superoxide. The experiments were carried out in triplicates on three distinct mitochondrial preparations.

pore-forming components, a core part formed either the F_1F_O-ATPase (Bonora et al., 2013; Mnatsakanyan et al., 2019; Urbani et al., 2019) and the adenine nucleotide translocator (ANT) (Karch et al., 2019; Neginskaya et al., 2019), both of which could be transformed into the high-conductance pore in response to higher mitochondrial matrix Ca^{2+} level (Neginskaya et al., 2022). Accordingly, it is possible that the mPTP consists of at least two pore-forming components. Moreover, the supramolecular organization of F_1F_O-ATPase with ANT plus phosphate carrier (PiC) in the ATP synthasome supercomplex is inversely related to mPTP formation. Cyclophilin D (CypD), a well-established positive regulator of the mPTP, appears to interact with all the components of the ATP synthasome destabilizing the supramolecular organization of the complexes and promoting the mPTP opening (Beutner et al., 2017). Conversely, HAP1 cell lines with vestigial ATP synthase (lacking of *g* and F6 subunit) are more sensitive to mPTP opening asserting that the F_1F_O-ATPase is not a component of mPTP but instead inhibits the pore opening (Pekson et al., 2023).

Phenolic phytochemicals, and in particular polyphenols, can prevent ATP hydrolysis by F_1 domain interaction without affecting the catalytic sites of the enzyme. F_1-ATPase is a motor protein that couples the rotation of its rotary γ subunit within a globular hexamer formed by non-catalytic sites on three α subunits alternate with three β subunits accommodating three catalytic sites. These compounds bind to distinct and unrelated regions in the hydrophobic area of the enzyme, which is where the C-terminal tip of the γ subunit contacts with the "bearing", a loop region, below the "crown region" of the α and β subunits (Gledhill et al., 2007). NRG, as a flavone belonging to the class of polyphenols, can inhibit the catalysis of ATP hydrolysis with higher selectivity towards Ca^{2+}-activated F_1F_O-ATPase than the enzyme in the presence of natural cofactor Mg^{2+}.

The mechanism of inhibition of F_1F_O-ATPase might be explained by NRG binding with F_1 domain. The NRG binding site is different from those of ATP and divalent cation cofactor (Mg^{2+} or Ca^{2+}). Interestingly, the F_1F_O-ATPase link to ATP is necessary to allow the interaction of NRG with the enzyme. Likely, the ATP binding change mechanism of F_1F_O-ATPase (Boyer, 2002) causes the appropriate conformational modification in the enzyme to guarantee the NRG binding. Otherwise, with respect to divalent cation, NRG has an affinity higher with F_1F_O-ATPase complexed with Mg^{2+} than with the enzyme-free, whereas NRG can displace F_1F_O-ATPase from binding to Ca^{2+} cofactor. Accordingly, the

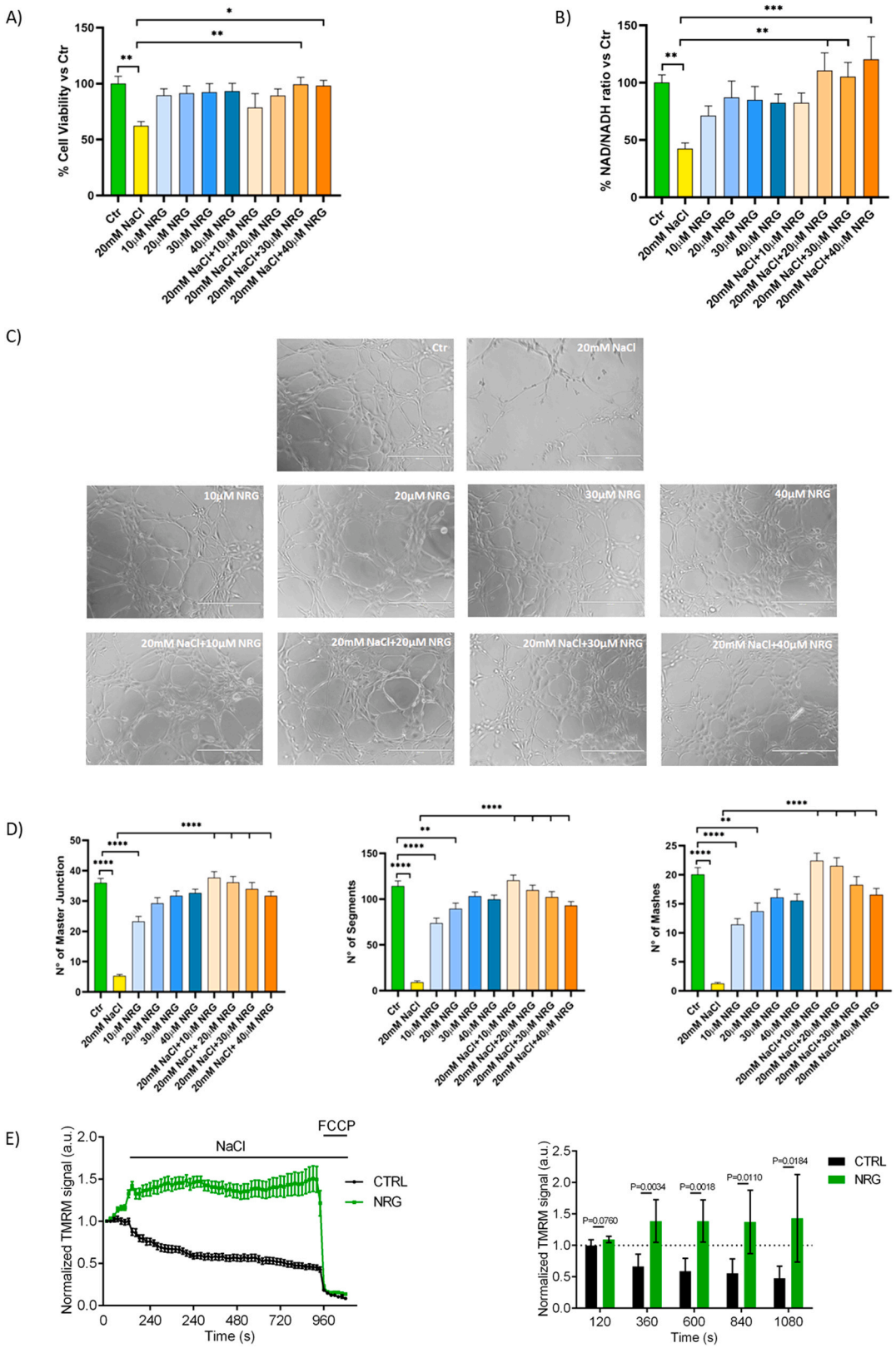

Fig. 7. Naringenin rescues cell viability and exerts beneficial effect on mitochondrial function and angiogenesis in SHRSP cerebral ECs exposed to high salt load. ECs were treated for 72 hrs with 20 mM NaCl either in the absence or in the presence of naringenin (from 10 to 40 μM). A) Evaluation of cell viability; N= 5. B) Evaluation of NAD/NADH ratio (as a measure of complex I activity) N= 4. C) Representative images of Matrigel assay and (D) the quantification of master junctions, segments, and mashes; N= 5. Ctr indicates untreated cells. * $P<0.05$, ** $P<0.01$, and *** $P<0.001$ were obtained using one-way ANOVA followed by Bonferroni post hoc analysis. Data are reported as mean±SEM. D) Kinetics of time-dependent changes in TMRM signal, upon addiction of 80 mM NaCl. 10 μM FCCP has been used as reference. Where indicated, cells were pre-treated with 40 μM naringenin (NRG) for 1 h. N = 4 independent experiments; mean±SEM. The bars in the graph (right panel) report the normalized TMRM values at different time points upon addiction of NaCl. N = 4 independent experiments; mean±SD.

inhibition of F_1F_O-ATPase by NRG before the activation by Ca^{2+} might suggest a protective role in the mPTP opening.

In all likelihood, the NRG interacts with the F_1 domain of the enzyme as highlighted by the inhibitory effect revealed on the F_1-ATPase activity and by the overlap of the binding site with QUE on the Ca^{2+}-activated F_1F_O-ATPase. The different effect of NRG on the enzyme activated by the two divalent cations has been speculated to be related to the different steric hindrance of ions since the Ca^{2+} has an atomic radius higher than Mg^{2+} (Casadio and Melandri, 1996; Nesci et al., 2018).

Homeostasis of Ca^{2+} and ROS production are regulated in mitochondria for maintaining cellular bioenergetics and metabolic precursor synthesis. However, pathological conditions, environmental conditions or injurious stimuli, causing mitochondrial dysfunction, promote the beginning and/or development of human diseases and the aging process (Harrington et al., 2023). The relevance of the underlying pathways causing mitochondrial impairment may aid in preventing various pathologies. mPTP opening is the biological event in mitochondria triggering different forms of regulated cell death (Izzo et al., 2016). The mPTP opening indicates that the IMM integrity has been lost, and mitochondria no longer maintain ion homeostasis. In all likelihood, mitochondrial dysfunction is counteracted by the NRG effect through two of its action features on mitochondrial biology. The negative role on the kinetics of Ca^{2+}-activated F_1F_O-ATPase blocks its bioarchitecture mechanism triggering the mPTP formation, whereas the antioxidant character of the molecular structure of NRG could have a scavenger effect on ROS production in mitochondria. NRG may possess the ability to arrest the feedforward loop supporting that an increase in Ca^{2+} and ROS activates the mPTP (Bauer and Murphy, 2020).

The ECs used in the present study were obtained from a known animal model of human hypertensive disease and related vascular damage, the SHRSP (Rubattu et al., 2016b). This model accelerates stroke occurrence when fed with a high salt/low potassium dietary regimen (Rubattu et al., 2016b, 1996). A severe mitochondrial complex I dysfunction due to Ndufc2 subunit inhibition was discovered as a major molecular mechanism underlying vascular damage and stroke predisposition in SHRSP (Rubattu et al., 2016a). We recently showed that primary cerebral ECs obtained from SHRSP pups represent a suitable experimental tool. Once exposed to a high salt load, they allow to dissect out the therapeutic effect of both chemical and natural substances able to counteract mitochondrial dysfunction (Algieri et al., 2022a; C. Algieri et al., 2023; Stanzione et al., 2023). In the current study, we provide consistent evidence by showing that NRG is able to counteract in a significant manner the high salt-induced injury in cerebral ECs, by strongly inhibits mPTP formation. Indeed, NRG preserved the mitochondrial membrane potential, and rescued both cell viability and endothelial cell tube formation, with a parallel recovery of complex I activity, in high salt-exposed ECs.

To sum up, the results have provided new knowledge on the mechanisms underlying cardiovascular protection by NRG through its impact on mitochondrial dysfunctions. In cellular models mimicking cardiovascular diseases with doxorubicin treatment, we highlighted a mitochondrial dysfunction counteracted by bergamot polyphenolic fraction (BPF) (Algieri et al., 2022b), which contains NRG. However, we can assert that, on high salt-exposed ECs predisposing to hypertension and onset of cardiovascular damage, BPF has a protective effect (Stanzione et al., 2023). It would be worthwhile to investigate the possibility that NRG, excluding the additive or synergistic action of other BPF polyphenols, could prevent mitochondrial dysfunction associated with cardiovascular diseases. The reduction of mPTP opening and the attenuation of oxidative stress may bring a great contribution in terms of efficacy and safety in the use of natural molecules to fight against major CVDs such as hypertension and its complications, the cardiac consequences of hyperglycemia, and ischemic heart disease, with the possibility of integrating or enhancing existing therapeutic strategies. Moreover, our results suggest that NRG represents a suitable approach to rescue endothelial function, through an improvement of mitochondrial function, in conditions of high salt-induced injury. Of note, NRG alone exerted a downregulatory effect on both complex I activity and the angiogenetic properties of the cells.

Fundings

This work was supported by the University of Bologna, grant numbers RFO 2021 to SN and an Alma Idea 2022 grant to SN; by a grant from the Italian Ministry of Health (Ricerca Corrente) to SR. The research leading to these results has also received funding from the European Union- NextGenerationEU through the Italian Ministry of University and Research under PNRR - M4C2-I1.3 Project PE_00000019 "HEAL ITALIA" to SR, CUP B53C22004000006. The views and opinions expressed are those of the authors only and do not necessarily reflect those of the European Union or the European Commission. Neither the European Union nor the European Commission can be held responsible for them.

CRediT authorship contribution statement

Salvatore Nesci: Conceptualization; Formal analysis; Funding acquisition; Supervision; Validation; Visualization; Writing - original draft. **Cristina Algieri:** Investigation. **Matteo Antonio Tallarida:** Formal analysis; Writing - Review & Editing. **Rosita Stanzione:** Investigation; Formal analysis. **Donatella Pietrangelo:** Methodology; Resources. **Fabiana Trombetti:** Methodology; Writing - Review & Editing. **Luca D'Ambrosio:** Resources. **Maurizio Forte:** Methodology. **Maria Cotugno:** Data Curation. **Rachele Bigi:** Writing - Review & Editing. **Loredana Maiuolo:** Writing - Review & Editing. **Antonio De Nino:** Writing - Review & Editing. **Saverio Marchi:** Writing - Review & Editing. **Paolo Pinton:** Writing - Review & Editing. **Giovanni Romeo:** Conceptualization; Writing - Review & Editing. **Speranza Rubattu:** Conceptualization; Funding acquisition; Supervision; Validation; Visualization; Writing - original draft.

Declaration of Competing Interest

The authors declare the following financial interests/personal relationships which may be considered as potential competing interests. Salvatore Nesci reports financial support was provided by University of Bologna, grant numbers RFO 2021 and Alma Idea 2022. Speranza Rubattu reports financial support was provided by Italian Ministry of Health Ricerca Corrente. Speranza Rubattu reports financial support was provided by Italian Ministry of University and Research PNRR - M4C2-I1.3 Project PE_00000019 "HEAL ITALIA", CUP B53C22004000006. If there are other authors, they declare that they have no known competing financial interests or personal relationships that could have appeared to influence the work reported in this paper.

Data availability

Data will be made available on request.

Acknowledgements

Danilo Matteuzzi and Roberto Giusti (Department of Veterinary Medical Sciences, University of Bologna) are gratefully acknowledged for kindly conferring swine hearts from a local abattoir to Biochemistry laboratories.

Appendix A. Supporting information

Supplementary data associated with this article can be found in the online version at doi:10.1016/j.ejcb.2024.151398.

References

Alavian, K.N., Beutner, G., Lazrove, E., Sacchetti, S., Park, H.-A., Licznerski, P., Li, H., Nabili, P., Hockensmith, K., Graham, M., Porter, G.A., Jonas, E.A., 2014. An uncoupling channel within the c-subunit ring of the F1FO ATP synthase is the mitochondrial permeability transition pore. Proc. Natl. Acad. Sci. U. S. A. 111, 10580–10585. https://doi.org/10.1073/pnas.1401591111.

Algieri, C., Trombetti, F., Pagliarani, A., Ventrella, V., Bernardini, C., Fabbri, M., Forni, M., Nesci, S., 2019. Mitochondrial Ca2+ -activated F1 FO -ATPase hydrolyzes ATP and promotes the permeability transition pore. Ann. N. Y. Acad. Sci. 1457, 142–157. https://doi.org/10.1111/nyas.14218.

Algieri, C., Trombetti, F., Pagliarani, A., Ventrella, V., Nesci, S., 2020. Phenylglyoxal inhibition of the mitochondrial F1FO-ATPase activated by Mg2+ or by Ca2+ provides clues on the mitochondrial permeability transition pore. Arch. Biochem. Biophys. 681, 108258 https://doi.org/10.1016/j.abb.2020.108258.

Algieri, C., Trombetti, F., Pagliarani, A., Ventrella, V., Nesci, S., 2021. The mitochondrial F1FO-ATPase exploits the dithiol redox state to modulate the permeability transition pore. Arch. Biochem Biophys. 712, 109027 https://doi.org/10.1016/j.abb.2021.109027.

Algieri, C., Bernardini, C., Oppedisano, F., La Mantia, D., Trombetti, F., Palma, E., Forni, M., Mollace, V., Romeo, G., Nesci, S., 2022a. Mitochondria bioenergetic functions and cell metabolism are modulated by the bergamot polyphenolic fraction. Cells 11, 1401. https://doi.org/10.3390/cells11091401.

Algieri, C., Bernardini, C., Oppedisano, F., La Mantia, D., Trombetti, F., Palma, E., Forni, M., Mollace, V., Romeo, G., Troisio, I., Nesci, S., 2022b. The impairment of cell metabolism by cardiovascular toxicity of doxorubicin is reversed by bergamot polyphenolic fraction treatment in endothelial cells. Int J. Mol. Sci. 23, 8977. https://doi.org/10.3390/ijms23168977.

Algieri, C., Bernardini, C., Marchi, S., Forte, M., Tallarida, M.A., Bianchi, F., La Mantia, D., Algieri, V., Stanzione, R., Cotugno, M., Costanzo, P., Trombetti, F., Maiuolo, L., Forni, M., De Nino, A., Di Nonno, F., Sciarretta, S., Volpe, M., Rubattu, S., Nesci, S., 2023. 1,5-disubstituted-1,2,3-triazoles counteract mitochondrial dysfunction acting on F1FO-ATPase in models of cardiovascular diseases. Pharmacol. Res. 187, 106561 https://doi.org/10.1016/j.phrs.2022.106561.

Algieri, V., Algieri, C., Maiuolo, L., De Nino, A., Pagliarani, A., Tallarida, M.A., Trombetti, F., Nesci, S., 2021. 1,5-Disubstituted-1,2,3-triazoles as inhibitors of the mitochondrial Ca2+ -activated F1 FO -ATP(hydrol)ase and the permeability transition pore. Ann. N. Y Acad. Sci. 1485, 43–55. https://doi.org/10.1111/nyas.14474.

Algieri, V., Algieri, C., Costanzo, P., Fiorani, G., Jiritano, A., Olivito, F., Tallarida, M.A., Trombetti, F., Maiuolo, L., De Nino, A., Nesci, S., 2023. Novel regioselective synthesis of 1,3,4,5-tetrasubstituted pyrazoles and biochemical valuation on F1FO-ATPase and mitochondrial permeability transition pore formation. Pharmaceutics 15, 498. https://doi.org/10.3390/pharmaceutics15020498.

Bauer, T.M., Murphy, E., 2020. Role of mitochondrial calcium and the permeability transition pore in regulating cell death. Circ. Res 126, 280–293. https://doi.org/10.1161/CIRCRESAHA.119.316306.

Beutner, G., Alanzalon, R.E., Porter, G.A., 2017. Cyclophilin D regulates the dynamic assembly of mitochondrial ATP synthase into synthasomes. Sci. Rep. 7, 14488 https://doi.org/10.1038/s41598-017-14795-x.

Bonora, M., Bononi, A., De Marchi, E., Giorgi, C., Lebiedzinska, M., Marchi, S., Patergnani, S., Rimessi, A., Suski, J.M., Wojtala, A., Wieckowski, M.R., Kroemer, G., Galluzzi, L., Pinton, P., 2013. Role of the c subunit of the FO ATP synthase in mitochondrial permeability transition. Cell Cycle 12, 674–683. https://doi.org/10.4161/cc.23599.

Bonora, M., Wieckowski, M.R., Sinclair, D.A., Kroemer, G., Pinton, P., Galluzzi, L., 2019. Targeting mitochondria for cardiovascular disorders: therapeutic potential and obstacles. Nat. Rev. Cardiol. 16, 33–55. https://doi.org/10.1038/s41569-018-0074-0.

Boyer, P.D., 2002. Catalytic site occupancy during ATP synthase catalysis. FEBS Lett. 512, 29–32. https://doi.org/10.1016/S0014-5793(02)02293-7.

Bradford, M.M., 1976b. A rapid and sensitive method for the quantitation of microgram quantities of protein utilizing the principle of protein-dye binding. Anal. Biochem. 72, 248–254.

Bradford, M.M., 1976a. A rapid and sensitive method for the quantitation of microgram quantities of protein utilizing the principle of protein-dye binding. Anal. Biochem. 72, 248–254. https://doi.org/10.1006/abio.1976.9999.

Carpentier, G., Berndt, S., Ferratge, S., Rasband, W., Cuendet, M., Uzan, G., Albanese, P., 2020. Angiogenesis analyzer for ImageJ - a comparative morphometric analysis of "Endothelial Tube Formation Assay" and "Fibrin Bead Assay". Sci. Rep. 10, 11568 https://doi.org/10.1038/s41598-020-67289-8.

Carresi, C., Gliozzi, M., Musolino, V., Scicchitano, M., Scarano, F., Bosco, F., Nucera, S., Maiuolo, J., Macrì, R., Ruga, S., Oppedisano, F., Zito, M.C., Guarnieri, L., Mollace, R., Tavernese, A., Palma, E., Bombardelli, E., Fini, M., Mollace, V., 2020. The effect of natural antioxidants in the development of metabolic syndrome: focus on bergamot polyphenolic fraction. Nutrients 12, 1504. https://doi.org/10.3390/nu12051504.

Casadio, R., Melandri, B.A., 1996. CaATP inhibition of the MgATP-dependent proton pump (H+-ATPase) in bacterial photosynthetic membranes with a mechanism of alternative substrate inhibition. JBIC 1, 284–291. https://doi.org/10.1007/s007750050055.

Cornish-Bowden, A., 1974. A simple graphical method for determining the inhibition constants of mixed, uncompetitive and non-competitive inhibitors. Biochem. J. 137, 143–144.

Forte, M., Schirone, L., Ameri, P., Basso, C., Catalucci, D., Modica, J., Chimenti, C., Crotti, L., Frati, G., Rubattu, S., Schiattarella, G.G., Torella, D., Perrino, C., Indolfi, C., Sciarretta, S., Italian Society of Cardiology Working group on Cellular and Molecular Biology of the Heart, 2021. The role of mitochondrial dynamics in cardiovascular diseases. Br J Pharmacol 178, 2060–2076. https://doi.org/10.1111/bph.15068.

Forte, M., Bianchi, F., Cotugno, M., Marchitti, S., De Falco, E., Raffa, S., Stanzione, R., Di Nonno, F., Chimenti, I., Palmerio, S., Pagano, F., Petrozza, V., Micaloni, A., Madonna, M., Relucenti, M., Torrisi, M.R., Frati, G., Volpe, M., Rubattu, S., Sciarretta, S., 2020. Pharmacological restoration of autophagy reduces hypertension-related stroke occurrence. Autophagy 16, 1468–1481. https://doi.org/10.1080/15548627.2019.1687215.

Giorgio, V., Burchell, V., Schiavone, M., Bassot, C., Minervini, G., Petronilli, V., Argenton, F., Forte, M., Tosatto, S., Lippe, G., Bernardi, P., 2017. Ca(2+) binding to F-ATP synthase β subunit triggers the mitochondrial permeability transition. EMBO Rep. 18, 1065–1076. https://doi.org/10.15252/embr.201643354.

Gledhill, J.R., Montgomery, M.G., Leslie, A.G.W., Walker, J.E., 2007. Mechanism of inhibition of bovine F1-ATPase by resveratrol and related polyphenols. Proc. Natl. Acad. Sci. U. S. A. 104, 13632–13637. https://doi.org/10.1073/pnas.0706290104.

Harrington, J.S., Ryter, S.W., Plataki, M., Price, D.R., Choi, A.M.K., 2023. Mitochondria in health, disease, and ageing. Physiol. Rev. https://doi.org/10.1152/physrev.00058.2021.

Heidary Moghaddam, R., Samimi, Z., Moradi, S.Z., Little, P.J., Xu, S., Farzaei, M.H., 2020. Naringenin and naringin in cardiovascular disease prevention: a preclinical review. Eur. J. Pharm. 887, 173535 https://doi.org/10.1016/j.ejphar.2020.173535.

Izzo, V., Bravo-San Pedro, J.M., Sica, V., Kroemer, G., Galluzzi, L., 2016. Mitochondrial permeability transition: new findings and persisting uncertainties. Trends Cell Biol. 26, 655–667. https://doi.org/10.1016/j.tcb.2016.04.006.

Karch, J., Bround, M.J., Khalil, H., Sargent, M.A., Latchman, N., Terada, N., Peixoto, P. M., Molkentin, J.D., 2019. Inhibition of mitochondrial permeability transition by deletion of the ANT family and CypD. Sci. Adv. 5, eaaw4597 https://doi.org/10.1126/sciadv.aaw4597.

Mnatsakanyan, N., Jonas, E.A., 2020. ATP synthase c-subunit ring as the channel of mitochondrial permeability transition: Regulator of metabolism in development and degeneration. J. Mol. Cell. Cardiol. 144, 109–118. https://doi.org/10.1016/j.yjmcc.2020.05.013.

Mnatsakanyan, N., Llaguno, M.C., Yang, Y., Yan, Y., Weber, J., Sigworth, F.J., Jonas, E. A., 2019. A mitochondrial megachannel resides in monomeric F1FO ATP synthase. Nat. Commun. 10, 5823. https://doi.org/10.1038/s41467-019-13766-2.

Mollace, V., Rosano, G.M.C., Anker, S.D., Coats, A.J.S., Seferovic, P., Mollace, R., Tavernese, A., Gliozzi, M., Musolino, V., Carresi, C., Maiuolo, J., Macrì, R., Bosco, F., Chiocchi, M., Romeo, F., Metra, M., Volterrani, M., 2021. Pathophysiological basis for nutraceutical supplementation in heart failure: a comprehensive review. Nutrients 13, 257. https://doi.org/10.3390/nu13010257.

Morris, G.M., Huey, R., Lindstrom, W., Sanner, M.F., Belew, R.K., Goodsell, D.S., Olson, A.J., 2009. AutoDock4 and AutoDockTools4: automated docking with selective receptor flexibility. J. Comput. Chem. 30, 2785–2791. https://doi.org/10.1002/jcc.21256.

Neginskaya, M.A., Solesio, M.E., Berezhnaya, E.V., Amodeo, G.F., Mnatsakanyan, N., Jonas, E.A., Pavlov, E.V., 2019. ATP synthase C-subunit-deficient mitochondria have a small cyclosporine A-sensitive channel, but lack the permeability transition pore. Cell Rep. 26, 11–17.e2. https://doi.org/10.1016/j.celrep.2018.12.033.

Neginskaya, M.A., Morris, S.E., Pavlov, E.V., 2022. Both ANT and ATPase are essential for mitochondrial permeability transition but not depolarization. iScience, 105447. https://doi.org/10.1016/j.isci.2022.105447.

Nesci, S., 2017. Mitochondrial permeability transition, F_1F_O-ATPase and calcium: an enigmatic triangle. EMBO Rep. 18, 1265–1267. https://doi.org/10.15252/embr.201744570.

Nesci, S., 2020. The mitochondrial permeability transition pore in cell death: a promising drug binding bioarchitecture. Med. Res. Rev. 40, 811–817. https://doi.org/10.1002/med.21635.

Nesci, S., 2022. What happens when the mitochondrial H+-translocating F1FO-ATP (hydrol)ase becomes a molecular target of calcium? The pore opens. Biochimie 198, 92–95. https://doi.org/10.1016/j.biochi.2022.03.012.

Nesci, S., Pagliarani, A., 2021b. Ca2+ as cofactor of the mitochondrial H+-translocating F1FO-ATP(hydrol)ase. Protein.: Struct., Funct., Bioinforma. 89, 477–482. https://doi.org/10.1002/prot.26040.

Nesci, S., Pagliarani, A., 2021a. Incoming news on the F-type ATPase structure and functions in mammalian mitochondria. BBA Adv. 1, 100001 https://doi.org/10.1016/j.bbadva.2020.100001.

Nesci, S., Ventrella, V., Trombetti, F., Pirini, M., Pagliarani, A., 2014b. Thiol oxidation is crucial in the desensitization of the mitochondrial F1FO-ATPase to oligomycin and other macrolide antibiotics. Biochim. Biophys. Acta 1840, 1882–1891. https://doi.org/10.1016/j.bbagen.2014.01.008.

Nesci, S., Ventrella, V., Trombetti, F., Pirini, M., Pagliarani, A., 2014a. The mitochondrial F1FO-ATPase desensitization to oligomycin by tributyltin is due to thiol oxidation. Biochimie 97, 128–137. https://doi.org/10.1016/j.biochi.2013.10.002.

Nesci, S., Trombetti, F., Ventrella, V., Pirini, M., Pagliarani, A., 2017. Kinetic properties of the mitochondrial F1FO-ATPase activity elicited by Ca(2+) in replacement of Mg (2+). Biochimie 140, 73–81. https://doi.org/10.1016/j.biochi.2017.06.013.

Nesci, S., Trombetti, F., Ventrella, V., Pagliarani, A., 2018. From the Ca2+-activated F1FO-ATPase to the mitochondrial permeability transition pore: an overview. Biochimie 152, 85–93. https://doi.org/10.1016/j.biochi.2018.06.022.

Nesci, S., Algieri, C., Trombetti, F., Ventrella, V., Fabbri, M., Pagliarani, A., 2021. Sulfide affects the mitochondrial respiration, the Ca2+-activated F1FO-ATPase activity and the permeability transition pore but does not change the Mg2+-activated F1FO-ATPase activity in swine heart mitochondria. Pharm. Res 166, 105495. https://doi.org/10.1016/j.phrs.2021.105495.

Nesci, S., Spagnoletta, A., Oppedisano, F., 2023. Inflammation, mitochondria and natural compounds together in the circle of trust. Int J. Mol. Sci. 24, 6106. https://doi.org/10.3390/ijms24076106.

Pekson, R., Liang, F.G., Axelrod, J.L., Lee, J., Qin, D., Wittig, A.J.H., Paulino, V.M., Zheng, M., Peixoto, P.M., Kitsis, R.N., 2023. The mitochondrial ATP synthase is a negative regulator of the mitochondrial permeability transition pore. Proc. Natl. Acad. Sci. U. S. A. 120, e2303713120 https://doi.org/10.1073/pnas.2303713120.

Penin, F., Godinot, C., Gautheron, D.C., 1979. Optimization of the purification of mitochondrial F1-adenosine triphosphatase. Biochim. Biophys. Acta 548, 63–71.

Pérez-Jiménez, J., Neveu, V., Vos, F., Scalbert, A., 2010. Identification of the 100 richest dietary sources of polyphenols: an application of the phenol-explorer database. Eur. J. Clin. Nutr. 64, S112–S120. https://doi.org/10.1038/ejcn.2010.221.

Perna, S., Spadaccini, D., Botteri, L., Girometta, C., Riva, A., Allegrini, P., Petrangolini, G., Infantino, V., Rondanelli, M., 2019. Efficacy of bergamot: from anti-inflammatory and anti-oxidative mechanisms to clinical applications as preventive agent for cardiovascular morbidity, skin diseases, and mood alterations. Food Sci. Nutr. 7, 369–384. https://doi.org/10.1002/fsn3.903.

Pinke, G., Zhou, L., Sazanov, L.A., 2020. Cryo-EM structure of the entire mammalian F-type ATP synthase. Nat. Struct. Mol. Biol. 27, 1077–1085. https://doi.org/10.1038/s41594-020-0503-8.

Rubattu, S., Volpe, M., Kreutz, R., Ganten, U., Ganten, D., Lindpaintner, K., 1996. Chromosomal mapping of quantitative trait loci contributing to stroke in a rat model of complex human disease. Nat. Genet 13, 429–434. https://doi.org/10.1038/ng0896-429.

Rubattu, S., Bianchi, F., Busceti, C.L., Cotugno, M., Stanzione, R., Marchitti, S., Di Castro, S., Madonna, M., Nicoletti, F., Volpe, M., 2015. Differential modulation of AMPK/PPARα/UCP2 axis in relation to hypertension and aging in the brain, kidneys and heart of two closely related spontaneously hypertensive rat strains. Oncotarget 6, 18800–18818. https://doi.org/10.18632/oncotarget.4033.

Rubattu, S., Di Castro, S., Schulz, H., Geurts, A.M., Cotugno, M., Bianchi, F., Maatz, H., Hummel, O., Falak, S., Stanzione, R., Marchitti, S., Scarpino, S., Giusti, B., Kura, A., Gensini, G.F., Peyvandi, F., Mannucci, P.M., Rasura, M., Sciarretta, S., Dwinell, M.R., Hubner, N., Volpe, M., 2016a. Ndufc2 gene inhibition is associated with mitochondrial dysfunction and increased stroke susceptibility in an animal model of complex human disease. J. Am. Heart Assoc. 5 https://doi.org/10.1161/JAHA.115.002701.

Rubattu, S., Stanzione, R., Volpe, M., 2016b. Mitochondrial dysfunction contributes to hypertensive target organ damage: lessons from an animal model of human disease. Oxid. Med Cell Longev. 2016, 1067801 https://doi.org/10.1155/2016/1067801.

Salehi, B., Fokou, P.V.T., Sharifi-Rad, M., Zucca, P., Pezzani, R., Martins, N., Sharifi-Rad, J., 2019. The therapeutic potential of naringenin: a review of clinical trials. Pharmaceuticals 12. https://doi.org/10.3390/ph12010011.

Sandoval-Acuña, C., Ferreira, J., Speisky, H., 2014. Polyphenols and mitochondria: an update on their increasingly emerging ROS-scavenging independent actions. Arch. Biochem Biophys. 559, 75–90. https://doi.org/10.1016/j.abb.2014.05.017.

Scalmani, G., Frisch, M.J., 2010. Continuous surface charge polarizable continuum models of solvation. I. General formalism. J. Chem. Phys. 132, 114110 https://doi.org/10.1063/1.3359469.

Stanzione, R., Forte, M., Cotugno, M., Oppedisano, F., Carresi, C., Marchitti, S., Mollace, V., Volpe, M., Rubattu, S., 2023. Beneficial effects of citrus bergamia polyphenolic fraction on saline load-induced injury in primary cerebral endothelial cells from the stroke-prone spontaneously hypertensive rat model. Nutrients 15, 1334. https://doi.org/10.3390/nu15061334.

Trott, O., Olson, A.J., 2009. AutoDock Vina: Improving the speed and accuracy of docking with a new scoring function, efficient optimization, and multithreading. J. Comput. Chem. https://doi.org/10.1002/jcc.21334.

Urbani, A., Giorgio, V., Carrer, A., Franchin, C., Arrigoni, G., Jiko, C., Abe, K., Maeda, S., Shinzawa-Itoh, K., Bogers, J.F.M., McMillan, D.G.G., Gerle, C., Szabò, I., Bernardi, P., 2019. Purified F-ATP synthase forms a Ca2+-dependent high-conductance channel matching the mitochondrial permeability transition pore. Nat. Commun. 10, 4341. https://doi.org/10.1038/s41467-019-12331-1.

Yonetani, T., 1982. [26] The Yonetani-Theorell graphical method for examining overlapping subsites of enzyme active centers, in: Purich, D.L. (Ed.), Methods in Enzymology, Enzyme Kinetics and Mechanism - Part C: Intermediates, Stereochemistry, and Rate Studies. Academic Press, pp. 500–509. https://doi.org/10.1016/S0076-6879(82)87028-6.

Zhao, Y., Truhlar, D.G., 2008. The M06 suite of density functionals for main group thermochemistry, thermochemical kinetics, noncovalent interactions, excited states, and transition elements: two new functionals and systematic testing of four M06-class functionals and 12 other functionals. Theor. Chem. Acc. 120, 215–241. https://doi.org/10.1007/s00214-007-0310-x.